ICAS 2020 SHANG HAI
International Council of the Aeronautical Sciences
32nd Congress of the International Council of the Aeronautical Sciences
September 6-10, 2021
Pudong Shangri-La, Shanghai, China

$\mathscr{L}_1$ ADAPTIVE CONTROL AUGMENTATION FOR A FLEXIBLE AIR-BREATHING HYPERSONIC VEHICLE MODEL

Chen Qi[1]

[1]China Aeronautical Radio Electronics Research Institute

Abstract

The longitudinal control of a flexible hypersonic vehicle model is investigated in this work. A baseline control scheme is designed with pole placement method to stabilize the vehicle model and to perform trajectory tracking. Thereafter, an augmentation system is developed with $\mathscr{L}_1$ adaptive control method to deal with the disturbances and system uncertainties as well as to improve the control performance. Simulations are conducted to validate the control designs in different scenarios. As the simulation results demonstrate, while both controllers show robustness to aerodynamic uncertainties, input disturbances, and parametric variations, the baseline controller suffers from control oscillations when reduced control surface functionality is introduced. The augmentation setup, however, successfully eliminates the oscillations and significantly improves the control performance. Furthermore, an analysis is carried out with the help of performance metrics. The augmentation scheme is shown to improve the tracking performance and enhance the robustness of the baseline control scheme. The contributions of this work include: the design of an augmentation system with the application of $\mathscr{L}_1$ adaptive control using modified piecewise constant adaptation laws for an air-breathing hypersonic vehicle model, and the comparison and analysis of its control performance with a conventional linear feedback control design.

Keywords: Flight control, adaptive control, pole placement, control augmentation, performance metric

1. Introduction

Prospects of feasible access to space and capability for prompt global strike have promoted the research and development of air-breathing hypersonic systems [1, 2, 3], and an ongoing effort is made by the aerospace community to achieve the goal of reliable and cost-effective hypersonic flights [1, 4]. Two failed attempts under DARPA's Falcon Project in 2011 indicated that traditional control designs applicable for subsonic and supersonic flights may pose problems for hypersonic flights [5]. Limited aerodynamic data, unknowns in the physical models, the peculiar structure of the propulsion system, as well as the harsh and uncertain operating conditions exhibit challenges to control designs [6].

Numerous control schemes and approaches have been proposed in the past twenty years. While the focus of earlier works was mainly on the design of linear robust controllers for linearized hypersonic vehicle models [8, 9, 10, 11, 12], the attention has shifted to nonlinear control designs for nonlinear models in recent years [13, 14, 15, 16, 17, 18, 19], and a variety of schemes have been explored to combat the design challenges, ranging from sliding mode control [20, 21, 22, 23], dynamic surface technique [24, 25, 26, 27], model predictive control [5, 28, 29, 30], backstepping method [31, 32, 33, 34, 35, 36], adaptive control [2, 24, 32, 37, 38], to schemes incorporating neural network method [38, 39, 40, 41, 42].

Since $\mathscr{L}_1$ adaptive control technique is employed in this work, a review of this method will be presented below.

The research on adaptive control began in the mid 1950s. Compared with the conventional robust control schemes, adaptive control requires less information in vehicle modeling. Furthermore, it is able to enhance the control performance when parametric variations, modeling uncertainties and actuation failures are present, hence making it a promising candidate for hypersonic flight control [43].

For hypersonic flight control, several adaptive schemes have been proposed. Fiorentini et al. [2] adopted nonlinear sequential loop closure method and adaptive dynamic inversion technique for the development of a robust adaptive control scheme. Daniel et al. [6] presented an study of adaptive control augmentation designs for a six-DoF hypersonic vehicle model, wherein a baseline controller was designed employing gain-scheduling and LQR-PI control law, and two model reference adaptive augmentation setups were examined: the first used a conventional open-loop reference model method, and the second applied a modified closed-loop reference model structure. A new approach was proposed by Su et al. [32] which combined the input shaping method and the constrained adaptive backstepping technique. Vibrations in the flexible dynamics was suppressed by implementing the input shaper outside of the feedback loop, and the constrained adaptive control law was formulated for reference trajectory tracking. Gao et al. [44] presented an adaptive fault-tolerant H_∞ controller design where an adaptive scheme was utilized to attenuate the external disturbance and cope with parameter uncertainties, as well as to reinforce the system robustness to sensor and actuator faults. Xu et al. [36] applied the command filter technique to design an adaptive back-stepping controller. Adaptive laws were utilized to cope with actuator faults, and auxiliary dynamics was used to deal with the input constraints.

Though adaptive control is an effective methodology to handle parametric uncertainties [45], it is a design challenge to find a proper trade-off between performance and robustness [46, 47]. Hovakimyan and Cao presented an $\mathscr{L}_1$ adaptive control scheme as an attempt to combat the challenge. Based on conventional model reference adaptive control structure, this scheme decouples adaptation from robustness, hence providing desired transient performance and guaranteed robustbess [47]. Several control designs using $\mathscr{L}_1$ adaptive control scheme have been proposed for hypersonic flight control. Lei et al. [48] presented an $\mathscr{L}_1$ adaptive control scheme for a flexible hypersonic vehicle model with unmodeled dynamics. The flexible vibrations was handled as unmodeled dynamics, and the $\mathscr{L}_1$ adaptive scheme was applied to compensate for the uncertainties. An $\mathscr{L}_1$ adaptive controller was proposed by Prime et al. [49] for the longitudinal dynamics of a hypersonic vehicle model. Simulation results demonstrated that despite some degradation in control performance, the stability of the controller was maintained in the presence of reduced control surface functionality, decreased longitudinal stability margins, and time delays. Banerjee et al. [37] proposed an $\mathscr{L}_1$ adaptive augmentation scheme for a hypersonic glider to perform a pull-up maneuver along its descent trajectory. The baseline controller was developed with dynamic pole placement method, and a piecewise constant $\mathscr{L}_1$ adaptive augmentation was made to cancel out the matched and unmatched uncertainties. Simulation results validated that the augmentation setup improved the control performance of the baseline scheme. However, the time delay margin of the system was reduced.

This paper presented a flight control scheme for the longitudinal dynamics of a flexible hypersonic vehicle model with uncertainties. A baseline control system is developed to perform trajectory tracking of velocity and flight path angle. Thereafter, an augmentation is made with an $\mathscr{L}_1$ adaptive scheme to cope with aerodynamic uncertainties, input disturbances, parametric variations, and reduced control surface functionality. Furthermore, a comparative study is made on the baseline controller and the $\mathscr{L}_1$ augmented scheme with respect to their performance.

The contributions of this work lies in: 1) the design of a pole placement control system that performs trajectory tracking for an air-breathing hypersonic vehicle model; 2) the implementation of the modified piecewise constant type $\mathscr{L}_1$ adaptive scheme to the baseline controller to cope with parametric variations and system uncertainties, and to improve the performance of the control scheme in the presence of reduced control functionality. Contrary to the work carried out by Banerjee et al. [37] where a similar baseline/augmentation approach is employed for a hypersonic glider, the augmentation setup developed in this work reposes upon a partition of the system dynamics, the vehicle model uses fuel equivalence ratio and elevator deflection angle to carry out both velocity and flight path angle tracking, therefore extending the application of $\mathscr{L}_1$ adaptive control in hypersonic flight control.

The paper is organized as follows: the second section depicts the vehicle model. The third section outlines the development of the proposed scheme. Simulation results are presented in the fourth section with an analysis on the control performance. Concluding remarks are offered in the last section.

2. Hypersonic vehicle model

The curve-fitted model [51] derived by Parker et al. is employed in the control design. It was developed from Bolender and Doman's full nonlinear longitudinal model [52] by substituting complex force and moment terms with curve-fit approximations. This model preserves the main characteristics of the richer model: structural flexibility, non-minimum phase behaviors and thrust to pitch moment coupling. The set of equations depicting the dynamics of the curve-fitted model reads as follows [51]:

$$\begin{aligned}
\dot{V} &= \frac{T\cos\alpha - D}{m} - g\sin\gamma \\
\dot{\gamma} &= \frac{L + T\sin\alpha}{mV} - \frac{g\cos\gamma}{V} \\
\dot{\theta} &= q \\
\dot{q} &= \frac{M + \tilde{\psi}_1\ddot{\eta}_1 + \tilde{\psi}_2\ddot{\eta}_2}{I_{yy}} \\
k_1\ddot{\eta}_1 &= -2\zeta_1\omega_1\dot{\eta}_1 - \omega_1^2\eta_1 + N_1 - \frac{\tilde{\psi}_1 M}{I_{yy}} - \frac{\tilde{\psi}_1\tilde{\psi}_2\ddot{\eta}_1}{I_{yy}} \\
k_2\ddot{\eta}_2 &= -2\zeta_2\omega_2\dot{\eta}_2 - \omega_2^2\eta_2 + N_2 - \frac{\tilde{\psi}_2 M}{I_{yy}} - \frac{\tilde{\psi}_2\tilde{\psi}_1\ddot{\eta}_2}{I_{yy}}
\end{aligned} \tag{1}$$

wherein the forces and moments are approximated as

$$\begin{aligned}
L &= \frac{1}{2}\rho V^2 S C_L(\alpha, \delta_e) \\
D &= \frac{1}{2}\rho V^2 S C_D(\alpha, \delta_e) \\
M &= z_T T + \frac{1}{2}\rho V^2 S\bar{c}\left[C_{M,\alpha}(\alpha) + C_{M,\delta_e}(\delta_e)\right] \\
T &= C_T^{\alpha^3}\alpha^3 + C_T^{\alpha^2}\alpha^2 + C_T^{\alpha}\alpha + C_T^0 \\
N_1 &= N_1^{\alpha^2}\alpha^2 + N_1^{\alpha}\alpha + N_1^0 \\
N_2 &= N_2^{\alpha^2}\alpha^2 + N_2^{\alpha}\alpha + N_2^0
\end{aligned} \tag{2}$$

and

$$\begin{aligned}
C_L(\alpha, \delta_e) &= C_L^{\alpha}\alpha + C_L^{\delta_e}\delta_e + C_L^0 \\
C_D(\alpha, \delta_e) &= C_D^{\alpha^2}\alpha^2 + C_D^{\alpha}\alpha + C_D^{\delta_e^2}\delta_e^2 + C_D^{\delta_e}\delta_e + C_D^0 \\
C_{M,\alpha}(\alpha) &= C_{M,\alpha}^{\alpha^2}\alpha^2 + C_{M,\alpha}^{\alpha}\alpha + C_{M,\alpha}^0 \\
C_{M,\delta_e}(\delta_e) &= c_e\delta_e \\
C_T^{\alpha^3} &= \beta_1\Phi + \beta_2 \\
C_T^{\alpha^2} &= \beta_3\Phi + \beta_4 \\
C_T^{\alpha} &= \beta_5\Phi + \beta_6 \\
C_T^0 &= \beta_7\Phi + \beta_8
\end{aligned} \tag{3}$$

The nomenclature is provided in Table 1, wherein S denotes reference, $\bar{c}$ designates mean aerodynamic chord, and z_T is the thrust to moment coupling coefficient.

The density of air ρ is calculated from the following exponential model [51]:

$$\rho = \rho_0 \exp[-(h - h_0)/h_s] \tag{4}$$

where ρ_0 denotes the nominal air density, h_0 the nominal altitude and h_s^{-1} is the decay rate of air density.

The engine dynamics takes the following form as a second-order system [51]:

$$\ddot{\Phi} = -2\zeta\omega\dot{\Phi} - \omega^2\Phi + \omega^2\Phi_c \tag{5}$$

Table 1 – List of states, inputs, and variables of the vehicle model.

Symbol	Definition
V	Velocity
γ	Fligt path angle
θ	Pitch angle
q	Pitch rate
η_i	ith generalized modal coordinate
$\dot{\eta}_i$	Time rate of change of ith generalized modal coordinate
Φ	Fuel-to-air ratio
δ_e	Elevator deflection
ρ	Density of air
S, $\bar{c}$, z_T	Geometric parameters
m	Vechicle mass
I_{yy}	Moment of inertia

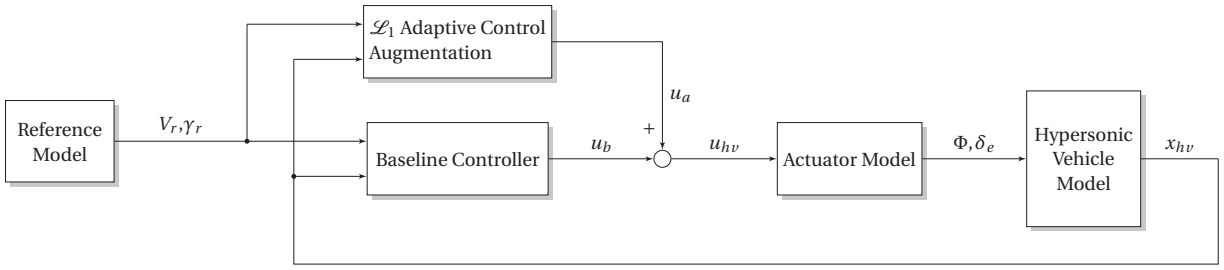

Figure 1 – Schematics of the proposed control design.

where Φ denotes the fuel-to-air ratio, Φ_c is the command signal, ω denotes the natural frequency of the engine dynamics, and ζ is the damping ratio.
The curve-fitted model comprises eight system states: $x_{hv} = [V, \gamma, \theta, q, \eta_1, \dot{\eta}_1, \eta_2, \dot{\eta}_2]^\top$, and two inputs: $u_{hv} = [\Phi, \delta_e]^\top$. In this work, we chose $y_{hv} = [V, \gamma]^\top$ as the controlled output. Interested readers could refer to the works of Parker et al. [51] and Bolender et al. [52] for additional details on this model.

3. Control development

This section presents the development of the proposed control design. The baseline controller is constructed with a pole placement method. Thereafter, an augmentation system with inner-loop and outer-loop architecture is designed with the modified piecewise constant type $\mathscr{L}_1$ adaptive control technique as presented by Li et al. [50] Figure 1 provides a schematic representation of the proposed scheme.

3.1 Baseline controller

The baseline controller is developed to stabilize the vehicle model and to perform basic tracking of the reference commands during flight.
The longitudinal dynamics presented by equation (1) could be rewritten into the following state-space representation:

$$\dot{\chi} = A_{hv}\chi + B_{hv}\Delta u_{hv} + F \tag{6}$$

where $\chi = [\Delta\theta, \Delta q, \Delta\gamma, \Delta V]^\top$ are perturbation state variables depicting deviation from the trim condition and $\Delta u_{hv} = [\Delta\Phi, \Delta\delta_e]^\top$ are increments of the control inputs to the trim values.

$$A_{hv} = \begin{bmatrix} 0 & 1 & 0 & 0 \\ M_\alpha & M_q & -M_\alpha & M_V \\ -N_\alpha & 0 & N_\alpha & N_V \\ -g + R_\alpha & 0 & -R_\alpha & R_V \end{bmatrix} \tag{7}$$

is the system matrix,

$$B_{hv} = \begin{pmatrix} 0 & 0 \\ M_\Phi & M_{\delta_e} \\ N_\Phi & N_{\delta_e} \\ R_\Phi & R_{\delta_e} \end{pmatrix} \tag{8}$$

is the input matrix, and

$$F = \begin{pmatrix} 0 \\ f_q \\ f_\gamma \\ f_V \end{pmatrix} \tag{9}$$

contains the residual terms (i.e. the higher order derivatives and the flexible states in the pitch rate dynamics). The expressions for the dimensional derivatives in A_{hv} and B_{hv} are provided in supplemental materials.
Applying pole placement technique yields the feedback gains:

$$K = \begin{pmatrix} K_V \\ K_\gamma \end{pmatrix}. \tag{10}$$

which render the closed-loop system matrix $A_{hv,cl} = A_{hv} - B_{hv}K$ Hurwitz and place the poles at the desired positions in the s plane.
Finally, the following baseline control law is applied to generate the control signals

$$\Delta u_b = -K\chi \tag{11}$$

Notice that in this study, both A_{hv} and B_{hv} are calculated at the trimmed cruising condition, therefore the resultant feedback gains are constant. The effectiveness of this simple strategy is validated by simulation results presented in the fourth section, where the vehicle model is commanded to track the reference signals of velocity and flight path angle in its flight profile. However, to cover a larger flight envelope, gain-scheduling or dynamic pole placement technique would be necessary for designing the baseline controller.

3.2 $\mathscr{L}_1$ adaptive augmentation

Owing to the uncertainties and disturbances that hypersonic vehicles are identified with, the baseline control design may not provide sufficient performance and robustness [6]. Therefore, an augmentation setup is designed and implemented in the current work. This section outlines the development of the augmentation setup.
A partition of the vehicle dynamics is first conducted, which determines the structure of the augmentation setup. Thereafter, an augmented controller is developed with $\mathscr{L}_1$ adaptive control technique.
The idea in designing the adaptive augmentation scheme is to treat the nonlinearities and disturbances as bounded perturbations, then apply $\mathscr{L}_1$ adaptive control method to estimate and attenuate the uncertainties [37]. Figure 2 provides a graphical representation of the $\mathscr{L}_1$ adaptive control scheme.

3.2.1 Partitioning of the system dynamics

In this work, a similar inner/outer loop architecture as that used by Tony et al. [53] is employed to design the augmentation system. First, the system is divided into two loops, where fuel-to-air ratio and pitch angle are utilized for the control of vehicle velocity and flight path angle. Thereafter, the required elevator deflection angle is obtained from the inner-loop as a real input to control the pitch dynamics. Figure 3 depicts the structure of the augmentation setup. The measured outputs V and γ, as well as the reference signals V_r and γ_r are used by the outer-loop to generate the signals of $\Phi_{c,a}$ and the virtual input θ_c. The actual control input $\delta_{e,a}$ is produced by the inner-loop. Below is an outline of this partitioning process.

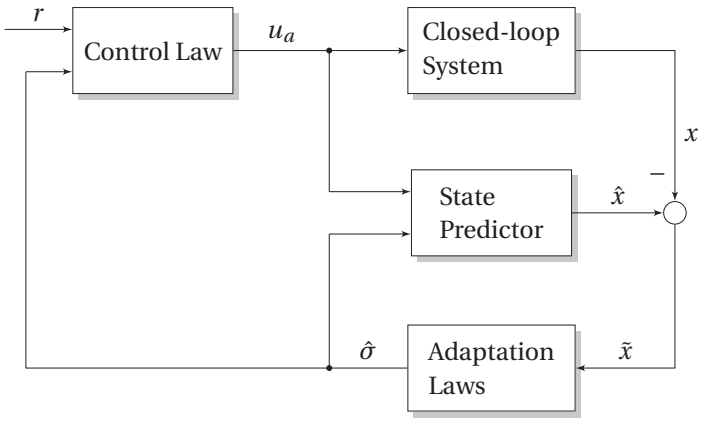

Figure 2 – Conceptual block diagram of the $\mathscr{L}_1$ adaptive control scheme.

The system presented in equation (1) can be partitioned into three subsystems [48]. First is the pitch dynamics

$$\begin{aligned} \dot{\theta} &= q \\ \dot{q} &= \frac{M + \tilde{\psi}_1 \ddot{\eta}_1 + \tilde{\psi}_2 \ddot{\eta}_2}{I_{yy}} \end{aligned} \tag{12}$$

The pitch rate dynamics could be rewritten as

$$\dot{q} = M_q q + M_{\delta_e} \delta_e + f_q^* \tag{13}$$

where δ_e is the control input and f_q^* denotes the nonlinearities.
Second is the flight path angle dynamics:

$$\begin{aligned} \dot{\gamma} &= \frac{L + T\sin\alpha}{mV} - \frac{g\cos\gamma}{V} \\ &= N_\alpha \gamma - N_\alpha \theta + f_\gamma^\star \end{aligned} \tag{14}$$

where $f_\gamma^\star$ denotes the nonlinearities and θ is utilized to control the flight path angle.
The third has the vehicle velocity:

$$\begin{aligned} \dot{V} &= \frac{T\cos\alpha - D}{m} - g\sin\gamma \\ &= R_V V + R_\Phi \Phi + f_V^\star \end{aligned} \tag{15}$$

where Φ is used to control the velocity dynamics and $f_V^\star$ is the nonlinearities.
Since the system output y_{hv} is expected to track the reference signals of V and γ, the outer-loop consists of the second and third subsystems, and outer-loop controllers are needed to determine the control signals of θ_c and $\Phi_{c,a}$. The pitch dynamics is considered as the inner-loop, and the signal of elevator deflection angel $\delta_{e,a}$ is generated by an inner-loop controller.

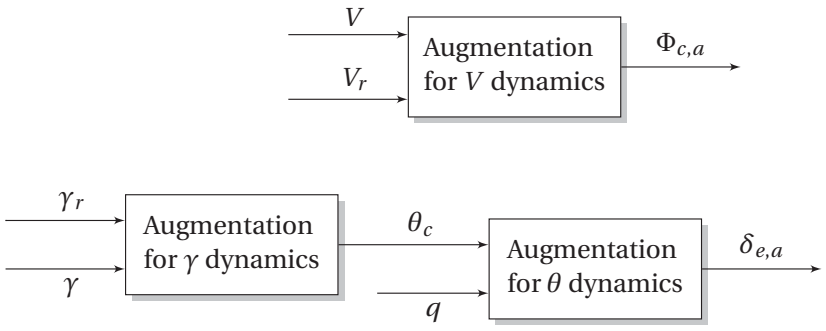

Figure 3 – Schematics of the augmentation system.

3.2.2 Outer-loop control design

Rewrite the flight path angle dynamics as follows

$$\dot{\gamma} = A_{m,\gamma}\gamma + b_\gamma(t)\left(\omega_\theta\theta + \frac{N_\alpha - A_{m,\gamma}}{b_\gamma(t)}\gamma + \frac{f_\gamma^\star}{b_\gamma(t)}\right) \tag{16}$$

where $A_{m,\gamma}$ specifies the desired closed-loop dynamics, $b_\gamma(t) = -N_\alpha$ is the input matrix, and ω_θ denotes the unknown input gain.

The control objective of the augmentation setup is to compensate for the uncertainties and ensure that γ tracks its reference signal.

As shown in Figure 2, the $\mathscr{L}_1$ adaptive controller comprises of three parts: a state predictor that estimates the system states, an adaptation law block that assesses the uncertainties, and a control law block that determines the control signals.

For the flight path angle augmentation, the following state predictor is considered:

$$\begin{aligned}\dot{\hat{\gamma}}(t) &= A_{m,\gamma}\hat{\gamma}(t) + b_\gamma(t)\left[\omega_{\theta,0}\theta_c(t) + \hat{\sigma}_\gamma(t)\right]\\ \hat{\gamma}(0) &= \gamma_0\end{aligned} \tag{17}$$

where $\omega_{\theta,0}$ is the nominal input gain, and the adaptive estimate $\hat{\sigma}_\gamma(t)$ is calculated from the modified piecewise constant adaptation algorithm [50] as follows:

$$\begin{aligned}h_\gamma(t) &= h_\gamma(kT_s)\\ \hat{\sigma}_\gamma(t) &= \hat{\sigma}_\gamma(kT_s),\ t \in [kT_s, (k+1)T_s]\\ h_\gamma(kT_s) &= -\tilde{\gamma}(kT_s) + h_\gamma[(k-1)T_s],\ h_\gamma(0) = 0\\ \hat{\sigma}_\gamma(kT_s) &= -\Phi_\gamma^{-1}(T_s)\mathbf{e}^{A_{m,\gamma}T_s}\tilde{\gamma}(kT_s)\\ &\quad + \Phi_\gamma^{-1}(T_s)h_\gamma(kT_s)\end{aligned} \tag{18}$$

for $k = 0, 1, 2, ...$, where

$$\Phi_\gamma(T_s) \triangleq A_{m,\gamma}^{-1}\left(\mathbf{e}^{A_{m,\gamma}T_s} - \mathbf{J}\right)b_\gamma(t), \tag{19}$$

$\mathbf{J}$ is a unit matrix, T_s is the adaptation sample period, and $\tilde{\gamma}(t) \triangleq \hat{\gamma}(t) - \gamma(t)$ is the difference between the estimated value and the actual value of γ. In this study, $T_s = 0.01$ s is set, corresponding to a sampling frequency of 100 Hz.

The control law is presented as follows:

$$\theta_c(s) = -k_\gamma D_\gamma(s)\left[\omega_{\theta,0}\theta_c(s) + \hat{\sigma}_\gamma(s) - k_{g,\gamma}(s)\gamma_r(s)\right] \tag{20}$$

where $\theta_c(s)$, $\hat{\sigma}_\gamma(s)$ and $\gamma_r(s)$ are Laplace transforms of the respective time domain signals; $k_\gamma \in \mathbb{R}^+$ is a feedback gain; $k_{g,\gamma}(s) \triangleq -1/\left(c_\gamma^\top A_{m,\gamma}^{-1}b_\gamma(t)\right)$ wherein $c_\gamma = 1$ is the output matrix of the γ dynamics; and transfer function $D_\gamma(s)$ is chosen to be strictly proper and it brings forth

$$C_\gamma(s) = \frac{\omega_\theta k_\gamma D_\gamma(s)}{1 + \omega_\theta k_\gamma D_\gamma(s)} \tag{21}$$

with $C_\gamma(0) = 1$, which is stable and strictly proper. The bandwidth of $C_\gamma(s)$ is selected in accordance with the uncertainty in the dynamics to attenuate the effect of the uncertainties.

Notice that the modified piecewise constant adaptive law was originally developed for LTI (linear time invariant) systems [50], however, the input matrix is taken as constant at every time step. Therefore, the control law could still be applied for the LTV augmentation scheme [37]. In this work, the dimensional derivative in the input matrix is calculated from the nondimensional derivatives given by equation (3).

Analogously, similar procedures are taken to design the augmentation scheme for the velocity channel, wherein $\Phi_{c,a}$ is utilized for velocity tracking.

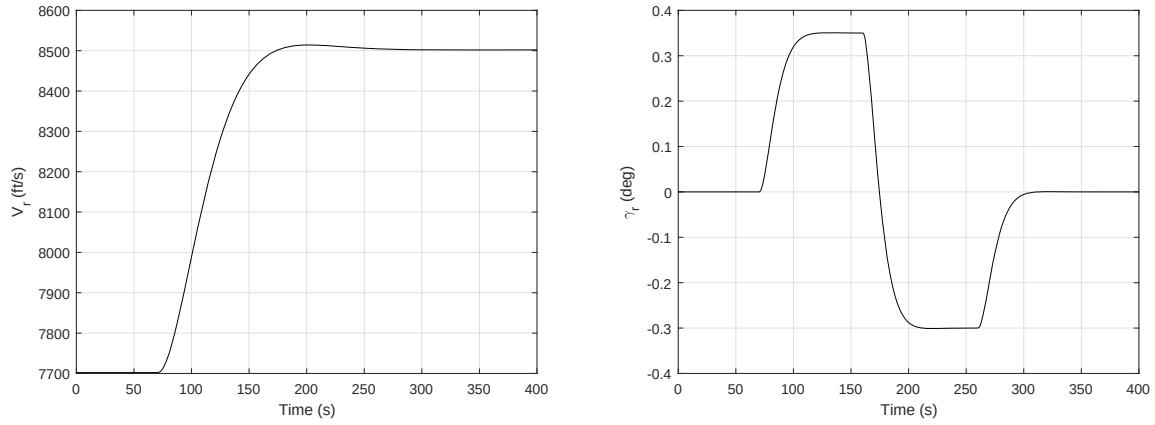

Figure 4 – Reference trajectories.

3.2.3 Inner-loop control design

Consider again the pitch rate dynamics given by equation (13). $\delta_{e,a}$ is used as the control input to ensure that $q_c = \dot{\theta}_c$ in the presence of uncertainties, where θ_c is the generated by the outer-loop.
The same control architecture as presented in the outer-loop control design is applied. Note that to ensure stability of the above $\mathscr{L}_1$ adaptive control designs, the choice of the feedback gains and the transfer functions $D(s)$ needs to meet the $\mathscr{L}_1$-norm condition [50]. For brevity, the definition of $\mathscr{L}_1$-norm will be omitted here.

4. Simulations

4.1 Simulation scenarios

The initial condition of the hypersonic vehicle model is $h = 85000$ ft and $V = 7702.0808$ ft/s, at trimmed cruising state. is used as an initial condition in the simulations. The reference trajectories are defined as follows: at time $t = 70$ s, there is an increase of 800 ft/s in the reference velocity, meanwhile the reference flight path angle increases by 0.35 deg; at $t = 70$ s and $t = 160$ s, changes in the reference flight path angle are -0.65 deg and $+0.3$ deg, respectively. The following filters are employed to smooth the aforementioned step changes [54]:

$$F_V(s) = \frac{\omega_{c1}}{s+\omega_{c1}} \frac{\omega_{c2}^2}{s^2+2\varepsilon_{c1}\omega_{c2}s+\omega_{c2}^2} \tag{22}$$

$$F_\gamma(s) = \frac{\omega_{c3}}{s+\omega_{c3}} \frac{\omega_{c4}^2}{s^2+2\varepsilon_{c2}\omega_{c4}s+\omega_{c4}^2} \tag{23}$$

with the following values assigned:

$$\omega_{c1} = 1, \quad \omega_{c2} = 0.04, \quad \varepsilon_{c1} = 0.8; \tag{24}$$

$$\omega_{c3} = 2, \quad \omega_{c4} = 0.12, \quad \varepsilon_{c2} = 0.9. \tag{25}$$

The reference trajectories are depicted in Figure 4. Note that the same test trajectories are employed throughout the simulations to simplify the comparison of results.
To verify the robustness of the proposed scheme, simulations are performed in five different scenarios. The first scenario examines the performance of the proposed controllers under nominal conditions, while the second investigates the robustness of the controllers with uncertainties introduced in the aerodynamic coefficients. The performance of the two schemes are evaluated in the third scenario with input disturbances added to the control inputs. In the fourth scenario, parametric variations are introduced to test the proposed control scheme. The fifth scenario evaluate the effectiveness of the controllers in the presence of reduced control functionality, whereas in the last scenario, all of the aforementioned issues are synthesized to assess the robustness of the control design. Note that in

each scenario, simulations are performed on both the baseline controller and the augmented control scheme, and the same implementation of the controllers are retained in all three scenarios.
The aforementioned time-varying uncertainties of the aerodynamic coefficients are presented in Table 2. The uncertain aerodynamic variables comprise lift coefficient, coefficient of δ_e contribution to lift coefficient, drag coefficient, coefficient of α contribution to moment coefficient, and the elevator pitching moment derivative. The aerodynamic uncertainties could be expressed by the following vector:

$$\mathbf{e} = \left[\varepsilon_{C_L^\alpha}, \varepsilon_{C_L^{\delta_e}} \varepsilon_{C_D^\alpha}, \varepsilon_{C_{M,\alpha}^\alpha}, \varepsilon_{C_M^{\delta_e}}\right]^\top \tag{26}$$

wherein each variable designates multiplicative uncertainty in the aerodynamic coefficient [37]. Each variable has unity nominal value and obeys a continuous normal distribution.
The input disturbances introduced in the third and last scenarios are generated as two signals obeying a continuous normal distribution, and are directly added to the control inputs before entering the actuator models. In this work, the three sigma limits set on the disturbances are as follows

$$\begin{aligned} \sigma_{\beta_c} &= [-0.06, 0.06] \\ \sigma_{\delta_e} &= [-0.2, 0.2] \end{aligned} \tag{27}$$

The parametric variations introduced in the fourth and the last scenario are displayed in Table 3. Variations in vehicle mass m, moment of inertia I_{yy}, reference area S, mean aerodynamic chord $\bar{c}$, and thrust to moment coupling coefficient z_T are considered, wherein both m and I_{yy} are assumed to be decreasing at a constant speed in the simulations, and each of the other three variables conforms to a continuous normal distribution with a designated error bound. In Table 3, t denotes the simulation time and T_{sim} is the time span of the simulation.
The reduced control functionality in the fifth and the last scenario is described by a ratio of actual control input to the commanded control value. Beginning from $t = 120$ s, the fuel-to-air ratio can only actuate 80% of the commanded value; and from $t = 200$ s on the elevators can only deflect 50% of the commanded angle.

4.2 Results and discussion

Simulation results of the controllers under nominal conditions are presented in Figure 5 and 6. As seen in Figure 5, while tracking errors of both controllers remain substantially small throughout the entire maneuver, the $\mathscr{L}_1$ augmented controller provides an improved tracking performance. Notably, at around $t = 70$ s when both velocity and flight path angle reference command are activated, the augmentation setup reduces both velocity and flight path angle tracking errors by 87.5%. A more detailed analysis on this improvement on control performance is provided in the next section.

Table 2 – Limits of the aerodynamic uncertainties.

Error vector elements	Error bounds (3σ limits)
$\varepsilon_{C_L^\alpha}$	$[0.3, 1.3]$
$\varepsilon_{C_L^{\delta_e}}$	$[0.3, 1.3]$
$\varepsilon_{C_D^\alpha}$	$[0.3, 1.3]$
$\varepsilon_{C_{M,\alpha}^\alpha}$	$[0.3, 1.3]$
$\varepsilon_{C_M^{\delta_e}}$	$[0.3, 1.3]$

Table 3 – Description of parametric variations.

Parameters	Time-varying changes
m	$m(t) = \left(1 - \frac{0.25}{T_{sim}} t\right) m_0$
I_{yy}	$I_{yy}(t) = \left(1 - \frac{0.25}{T_{sim}} t\right) I_{yy,0}$
S	$S(t) = \varepsilon_S S_0, \quad \varepsilon_S \in [0.8, 1.2]$
$\bar{c}$	$\bar{c}(t) = \varepsilon_{\bar{c}} \bar{c}_0, \quad \varepsilon_{\bar{c}} \in [0.8, 1.2]$
z_T	$z_T(t) = \varepsilon_{z_T} z_{T,0}, \quad \varepsilon_{z_T} \in [0.8, 1.2]$

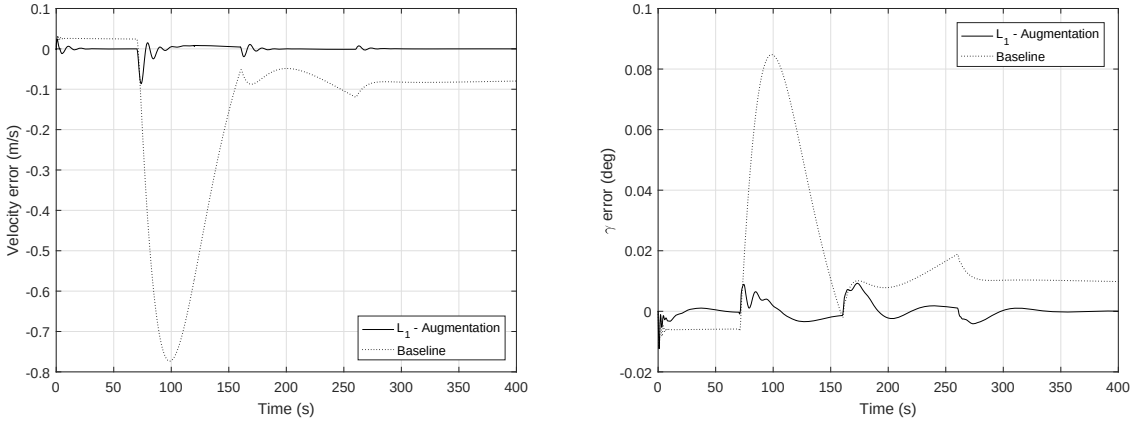

Figure 5 – Tracking errors: nominal conditions.

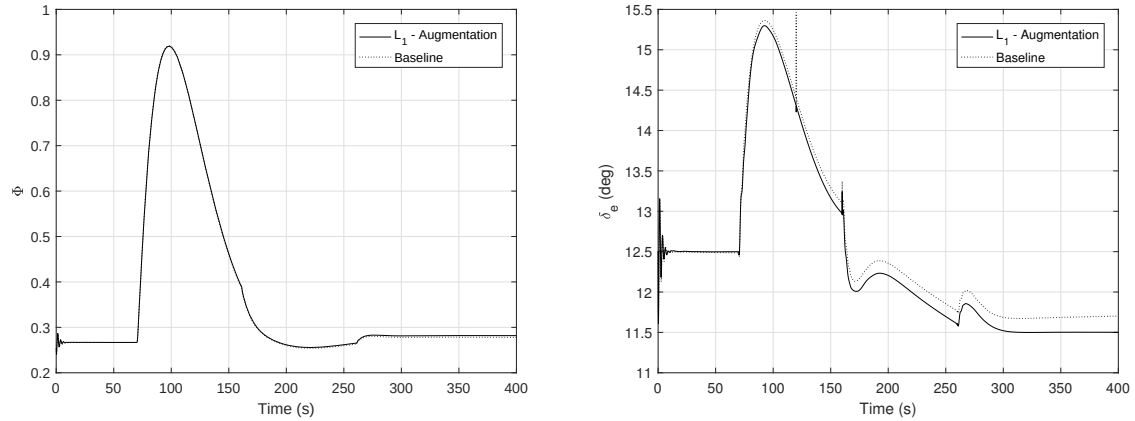

Figure 6 – Control inputs: nominal conditions.

Figure 6 shows the time history of the control signals under the nominal conditions. A considerable initial control effort can be observed in the plots, which is spent to trim the model. Overall, both control inputs remain stable and well behaved during the whole simulation phase.
Figure 7 shows the tracking error behavior of the control schemes in the second scenario. Oscillations in the tracking error plots reveals the effect of the aerodynamic uncertainties. The tracking performance is retained compared with Figure 5 and the augmentation system again is shown to enhance the tracking performance. The control inputs are plotted in Figure 8. Mild oscillations are visible in the plots, showing the effects of the aerodynamic uncertainties.
Figure 9 and Figure 10 show the simulation results of the third test case. Both schemes are affected by the input disturbances, and the $\mathscr{L}_1$ augmented scheme still attains an improved performance than the baseline scheme.
The performance of the control schemes in the fourth scenario are shown in Figure 11 and Figure 12. As shown in the plots, both baseline and augmented scheme retain their tracking performance in the presence of parametric variations, and a reduction in control energy can be observed near the end of the simulation, since the vehicle mass and moment of inertia decrease with time in this scenario.
Figure 13 and 14 show the performance of the schemes when reduced control functionality is present. It is observed that in the baseline case the control loss of elevators activated at $t = 200$ s induces oscillations in the control inputs and tracking variables, and the system gradually enters into an unstable state. However, with the $\mathscr{L}_1$ augmentation system implemented, the control oscillations provoked by reduced control functionality are suppressed, and the oscillations in V and γ are also eliminated. The fifth test case therefore demonstrates that with reduced control functionality, the augmented controller

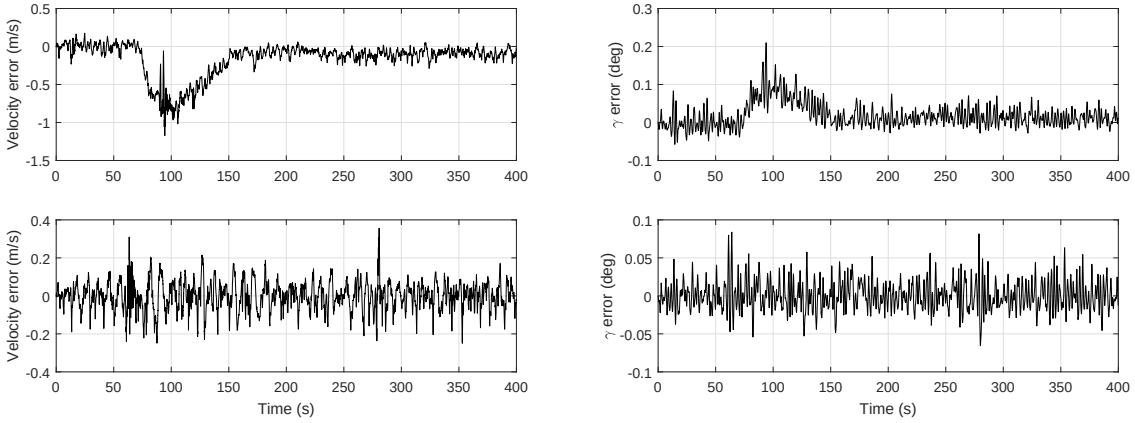

Figure 7 – Tracking error plots: aerodynamic uncertainties. (Above: baseline, below: $\mathscr{L}_1$ augmented.)

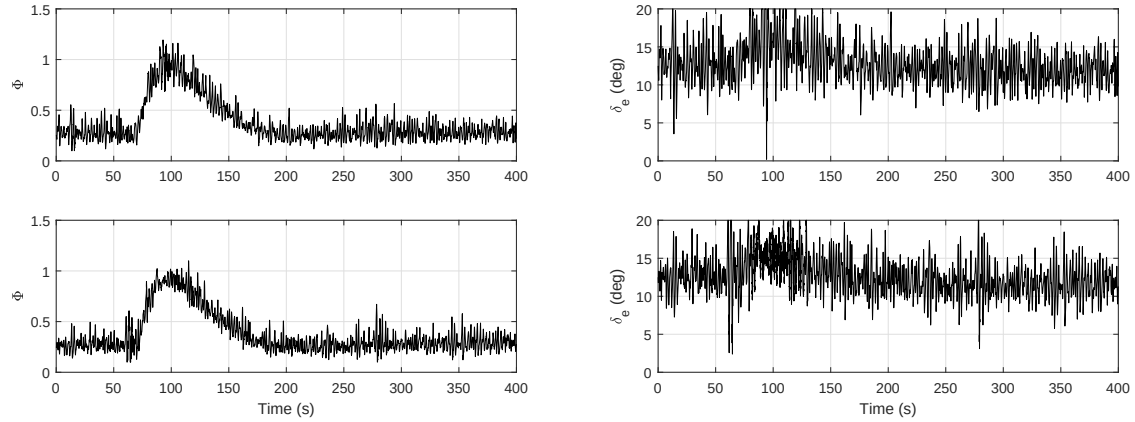

Figure 8 – Control inputs: aerodynamic uncertainties. (Above: baseline, below: $\mathscr{L}_1$ augmented.)

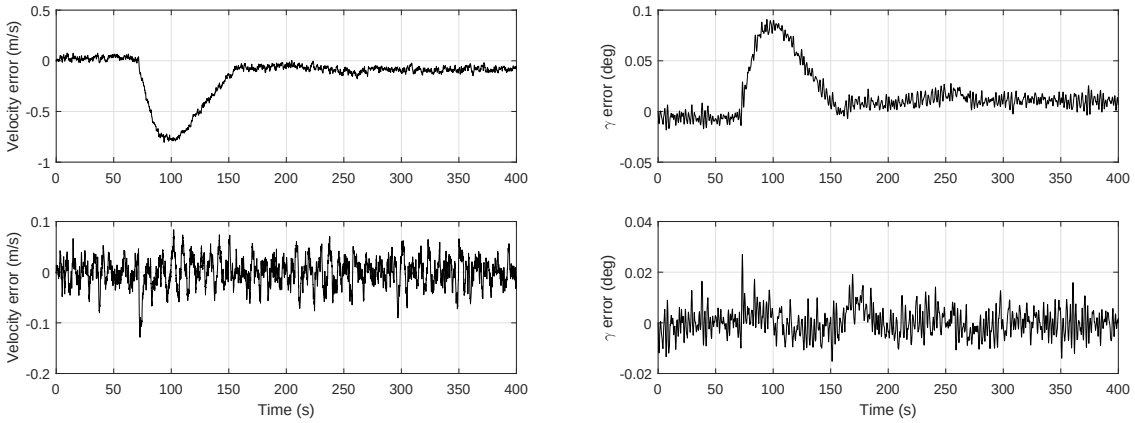

Figure 9 – Tracking error plots: input disturbances. (Above: baseline, below: $\mathscr{L}_1$ augmented.)

is able to inhibit control chattering and improve the performance of the baseline controller.
Figure 15 and 16 depict the performance of the schemes in the case of combined uncertainties. Oscillations could be seen in both control inputs and tracking errors of both controllers. And the adaptive augmentation improves the overall control performance of the baseline scheme in this scenario.

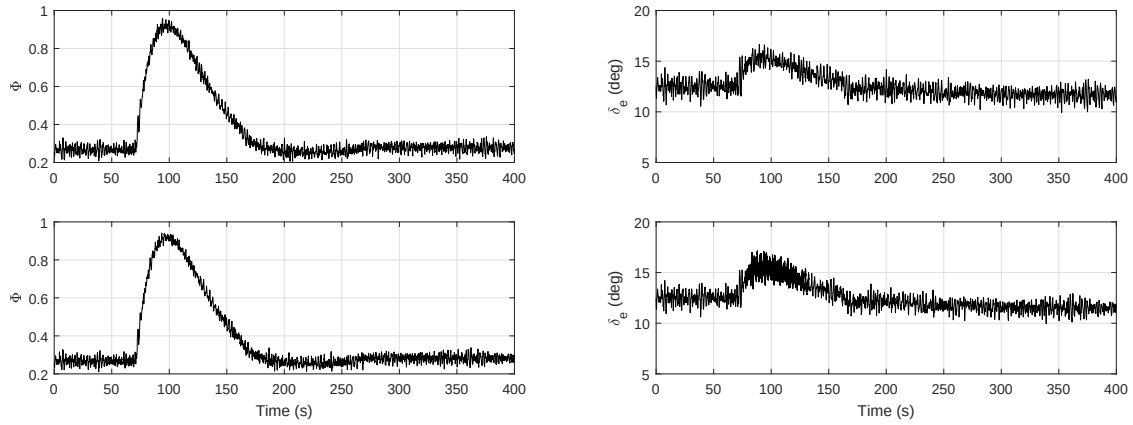

Figure 10 – Control inputs: aerodynamic uncertainties. (Above: baseline, below: $\mathscr{L}_1$ augmented.)

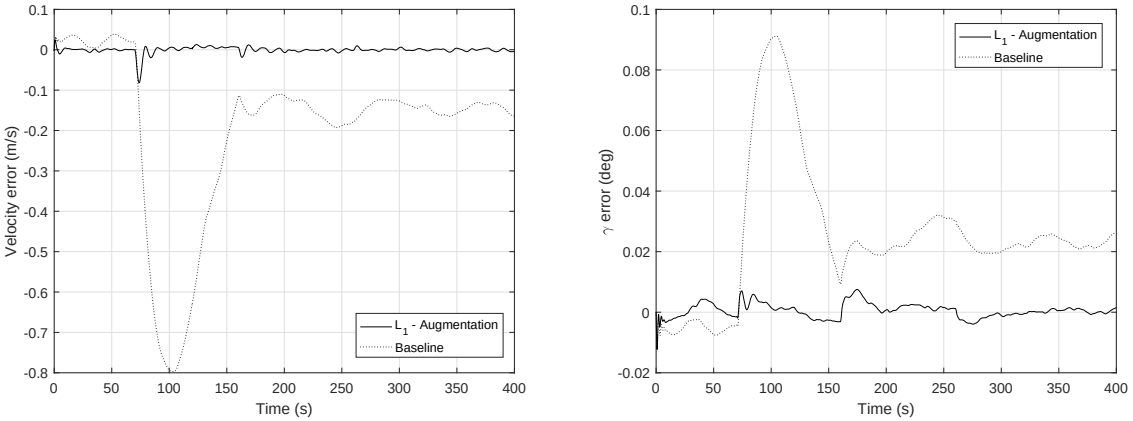

Figure 11 – Tracking error plots: parametric variations.

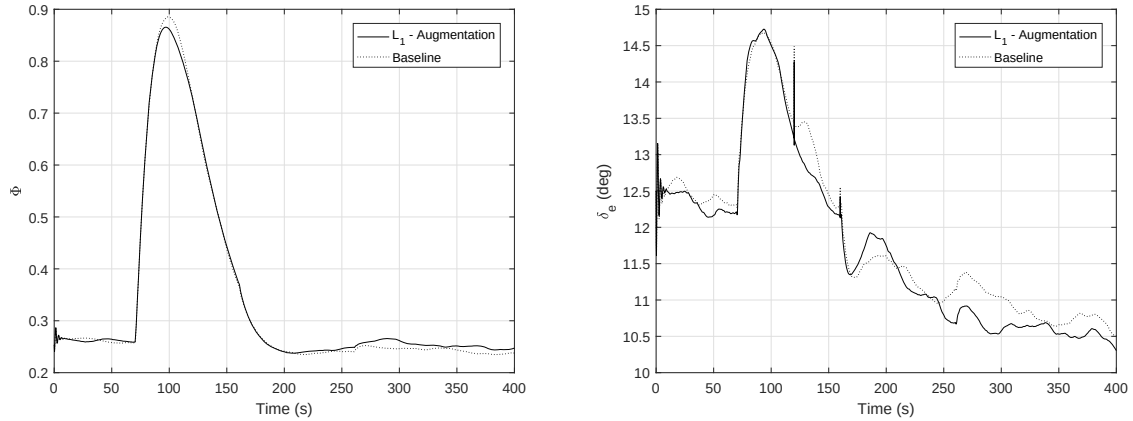

Figure 12 – Control inputs: parametric variations.

4.3 Performance analysis

This section gives an analysis and a comparison on the performance of the two control methodologies employed in this study.

First, use the error dynamics and its acceleration to assess the performance of the baseline controller and the augmented scheme. As shown by Figure 5, 7, 11, 13 and 15, for all the six simulation

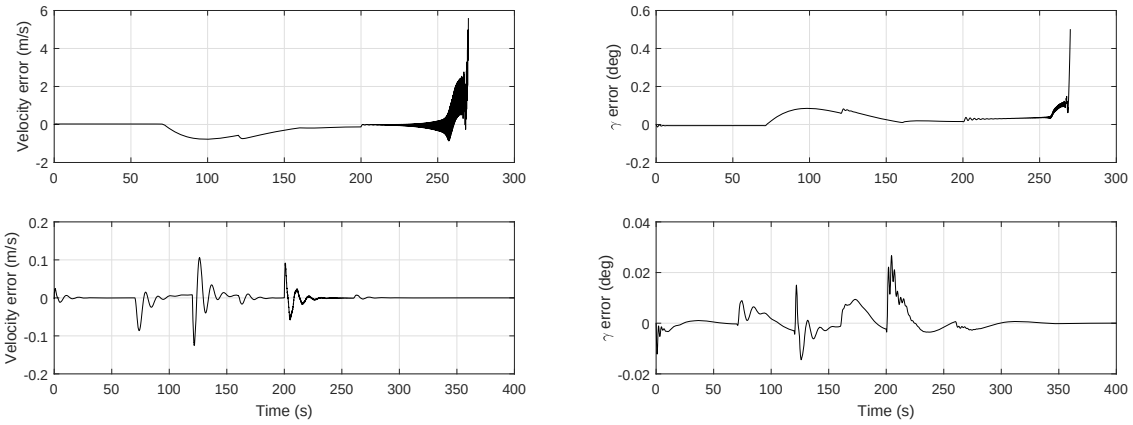

Figure 13 – Tracking error plots: reduced control functionality. (Above: baseline, below: $\mathscr{L}_1$ augmented.)

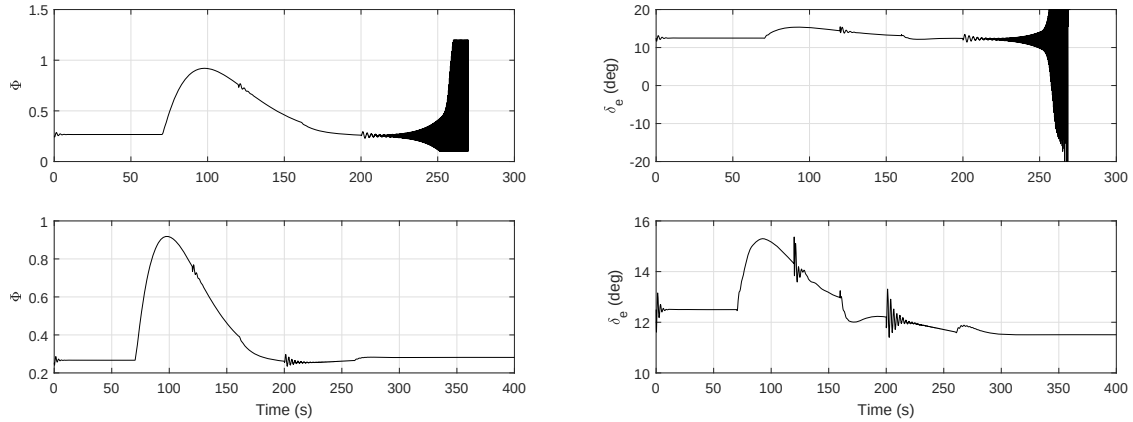

Figure 14 – Control inputs: aerodynamic uncertainties and reduced control functionality. (Above: baseline, below: $\mathscr{L}_1$ augmented.)

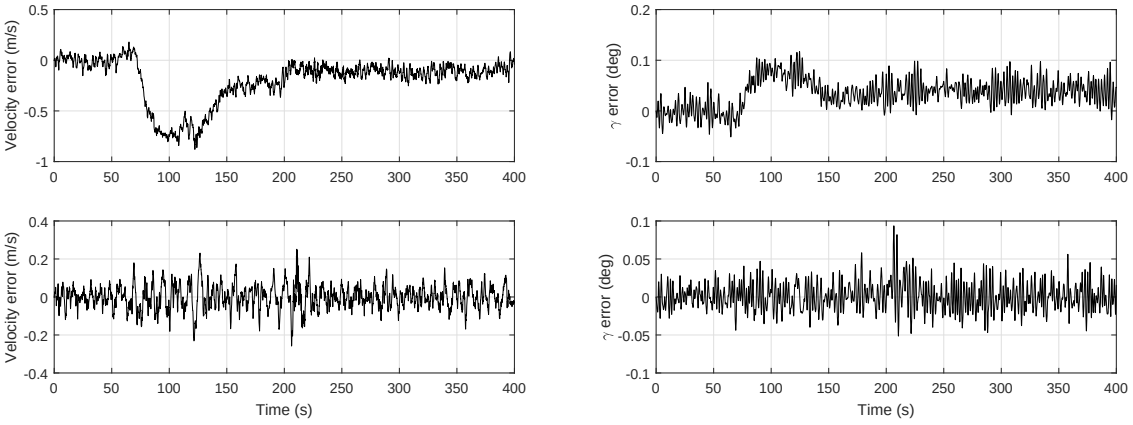

Figure 15 – Tracking error plots: combined uncertainties. (Above: baseline, below: $\mathscr{L}_1$ augmented.)

scenarios the error dynamics of the $\mathscr{L}_1$ augmented controller converges to zero more rapidly than that of the baseline controller. This indicates an improvement to the settling time brought by the augmentation system.

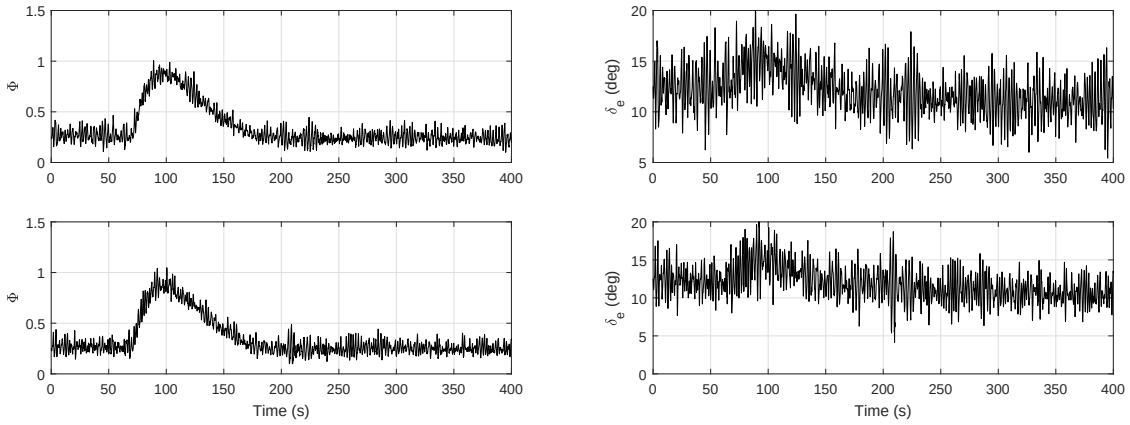

Figure 16 – Control inputs: combined uncertainties. (Above: baseline, below: $\mathscr{L}_1$ augmented.)

Table 4 – Comparison of performance metrics: $E_{\mathscr{L}_\infty}$

Simulation scenario	Tracking variable	Baseline	Augmented
Scenario I	V	0.773	0.0862
	γ	0.0848	0.0122
Scenario II	V	1.17	0.356
	γ	0.210	0.0838
Scenario III	V	0.805	0.128
	γ	0.0909	0.0271
Scenario IV	V	0.797	0.0817
	γ	0.0912	0.0121
Scenario V	V	/	0.126
	γ	/	0.0267
Scenario VI	V	0.880	0.258
	γ	0.117	0.0936

Second, the following metrics are used for comparison of the tracking performance between the baseline to the $\mathscr{L}_1$ augmented control scheme [46]:

$$E_{\mathscr{L}_\infty} = \max_{t\in[t_0,t_f]} \left|\psi - \psi_{ref}\right|$$
$$E_{\mathscr{L}_2} = \sqrt{\int_{t_0}^{t_f} (\psi - \psi_{ref})^2\, dt} \tag{28}$$

where ψ denotes the tracking variable considered, $E_{\mathscr{L}_\infty}$ evaluates the maximum values of tracking error and $E_{\mathscr{L}_2}$ is a measure of its energy. For both metrics, a smaller value means a better tracking performance.

Table 4 and 5 present the performance metrics obtained from the simulation results. Note that the error norms of the baseline scheme in the fifth scenario where reduced control functionality is introduced are not recorded since the vehicle model becomes unstable in the simulations.

The following conclusion could be drawn from the results outlined in Table 4 and 5: 1) The augmentation system enhances the tracking performance of the baseline controller, and 2) the fifth scenario shows the most significant improvement by the adaptive augmentation, where the $\mathscr{L}_1$ adaptive controller successfully inhibits chattering in the control channel and stablizes the vehicle model in the case of reduced control functionality.

5. Conclusion

This work presents the development of a control design for a flexible hypersonic vehicle model. The pole placement technique is applied to design the baseline scheme, and the augmentation system is implemented to cancel out the uncertainties. The design of the augmentation setup bases upon

Table 5 – Comparison of performance metrics: $E_{\mathscr{L}_2}$

Simulation scenario	Tracking variable	Baseline	Augmented
Scenario I	V	5.05	0.180
	γ	0.552	0.0540
Scenario II	V	5.38	1.46
	γ	0.733	0.383
Scenario III	V	5.08	0.543
	γ	0.562	0.104
Scenario IV	V	5.66	0.177
	γ	0.688	0.0493
Scenario V	V	/	0.340
	γ	/	0.0844
Scenario VI	V	5.88	1.24
	γ	0.914	0.363

partitioning of the model dynamics and three modified piecewise constant type $\mathscr{L}_1$ adaptive controllers are utilized to manage the uncertainties and improve the control performance. Simulations are performed in six different scenarios. Both baseline and augmented controllers shows robustness to aerodynamic uncertainties, input disturbances, and parametric variations, however, the augmentation system achieves better tracking performance. In the scenario where the vehicle model experiences reduced control functionality, the baseline controller could not handle the oscillations induced in the control channel and the system becomes unstable; the augmentation system on the contrary successfully attenuates the oscillations and stablizes the vehicle model. From the evaluation of tracking performance and control inputs behaviors, it could be concluded that the augmentation setup achieves improved performance and robustness in the presence of uncertainties. Future work is to extend the proposed approach to the control of the whole flight envelop, and a 6-DOF hypersonic vehicle model will be employed to include the lateral dynamics and control.

Appendix

Expressions for the elements of the vector fields defined in equation (7) and equation (8) are as follows:

Elements in matrix A_{hv}:

$$
\begin{aligned}
M_\alpha &= \frac{1}{I_{yy}}\left[z_T\left(3C_T^{\alpha^3}\alpha^2+2C_T^{\alpha^2}\alpha+C_T^{\alpha}\right)\right.\\
&\qquad \left.+\bar{q}S\bar{c}\left(2C_{M,\alpha}^{\alpha^2}\alpha+C_{M,\alpha}^{\alpha}\right)\right]\\
M_q &= 0\\
M_V &= \frac{1}{I_{yy}}\rho V S\bar{c}\left[C_{M,\alpha}(\alpha)+C_{M,\delta_e}(\delta_e)\right]
\end{aligned}
$$

$$
\begin{aligned}
N_\alpha &= \frac{1}{mV}\left(-\frac{\partial T}{\partial \alpha}\sin\alpha - T\cos\alpha - \bar{q}SC_L^{\alpha}\right)\\
N_V &= \frac{1}{mV^2}T\sin\alpha - \frac{\rho S}{2m}C_L(\alpha,\delta_e) - \frac{g}{V^2}\cos\gamma\\
R_\alpha &= \frac{1}{m}\left[\frac{\partial T}{\partial \alpha}\cos\alpha - T\sin\alpha - \bar{q}S\left(2C_D^{\alpha^2}\alpha+C_D^{\alpha}\right)\right]\\
&\qquad +g\cos\gamma\\
R_V &= -\frac{1}{m}\rho V S C_D(\alpha,\delta_e)
\end{aligned}
$$

Elements in matrix B_{hv}:

$$M_\Phi = \frac{z_T}{I_{yy}}\left(\beta_1\alpha^3 + \beta_3\alpha^2 + \beta_5\alpha + \beta_7\right)$$
$$M_{\delta_e} = \frac{1}{I_{yy}}\bar{q}S\bar{c}c_e$$
$$N_\Phi = -\frac{1}{mV}\frac{\partial T}{\partial \Phi}\sin\alpha$$
$$N_{\delta_e} = -\frac{1}{mV}\bar{q}SC_L^{\delta_e}$$

$$R_\Phi = \frac{1}{m}\frac{\partial T}{\partial \Phi}\cos\alpha$$
$$R_{\delta_e} = -\frac{\bar{q}S}{m}\left(2C_D^{\delta_e^2}\delta_e + C_D^{\delta_e}\right)$$

where $\bar{q} = \frac{1}{2}\rho V^2$, denoting dynamic pressure.

References

[1] Fiorentini L, Serrani A, Bolender M, et al. Robust nonlinear sequential loop closure control design for an air-breathing hypersonic vehicle model. *American Control Conference*, Washington. 2008; 3458-63.

[2] Fiorentini L, Serrani A, Bolender M, et al. Nonlinear Robust Adaptive Control of Flexible Air-Breathing Hypersonic Vehicles. *Journal of Guidance, Control, and Dynamics*. 2009; 32: 402-17.

[3] Echols J, Puttannaiah K, Mondal K, et al. Fundamental Control System Design Issues for Scramjet-Powered Hypersonic Vehicles. *AIAA Guidance, Navigation, and Control Conference*. Kissimmee, Florida, 2015. AIAA-2015-1760.

[4] Chen Q, Wan J, and Ai J. $\mathscr{L}_1$ adaptive controller design for hypersonic formation flight. *Science China Technological Sciences*. 2016; 59: 1597-608.

[5] Christopher P, Morgan B, and Ilya K. Model Predictive Control Guidance with Extended Command Governor Inner-Loop Flight Control for Hypersonic Vehicles. *AIAA Guidance, Navigation, and Control Conference*, Boston, 2013. AIAA-2013-5028.

[6] Daniel P, Anuradha M, Jonathan A, et al. Adaptive Control of a Generic Hypersonic Vehicle. *AIAA Guidance, Navigation, and Control Conference*, Boston, 2013. AIAA-2013-4514.

[7] Preller D and Smart M. Longitudinal Control Strategy for Hypersonic Accelerating Vehicles. *Journal of Spacecraft and Rockets*. 2015; 52: 993-8.

[8] Buschek H and Calise A. Uncertainty modeling and fixed-order controller design for a hypersonic vehicle model. *Journal of Guidance, Control, and Dynamics*. 1997; 20: 42-8.

[9] Chavez F and Schmidt D. Uncertainty modeling for multivariable-control robustness analysis of elastic high-speed vehicles. *Journal of Guidance, Control, and Dynamics*. 1999; 22: 87-95.

[10] Lind R. Linear parameter-varying modeling and control of structural dynamics with aerothermoelastic effects. *Journal of Guidance, Control, and Dynamics*. 2002; 25: 733-9.

[11] Sigthorsson D, Jankovsky P, Serrani A, et al. Robust linear output feedback control of an airbreathing hypersonic vehicle. *Journal of Guidance, Control, and Dynamics*. 2008; 31: 1052-66.

[12] Li H, Si Y, Wu L, et al. Guaranteed cost control with poles assignment for a flexible air-breathing hypersonic vehicle. *International Journal of Systems Science*. 2011; 42: 863-76.

[13] Fiorentini L, Serrani A, Bolender M, et al. Nonlinear Control of Non-minimum Phase Hypersonic Vehicle Models. *American Control Conference*, Vols 1-9. 2009: 3160-5.

[14] Wilcox Z, MacKunis W, Bhat S, et al. Lyapunov-Based Exponential Tracking Control of a Hypersonic Aircraft with Aerothermoelastic Effects. *Journal of Guidance, Control, and Dynamics*. 2010; 33: 1213-24.

[15] Sun H, Yang Z and Zeng J. New Tracking-Control Strategy for Airbreathing Hypersonic Vehicles. *Journal of Guidance, Control, and Dynamics*. 2013; 36: 846-59.

[16] Yang J, Li S, Sun C, et al. Nonlinear-Disturbance-Observer-Based Robust Flight Control for Airbreathing Hypersonic Vehicles. *IEEE Transactions on Aerospace and Electronic Systems*. 2013; 49: 1263-75.

[17] Zhang Y and Xian B. Continuous nonlinear asymptotic tracking control of an air-breathing hypersonic vehicle with flexible structural dynamics and external disturbances. *Nonlinear Dynamics*. 2015; 83: 867-91.

[18] An H, Liu J, Wang C, et al. Disturbance Observer-Based Antiwindup Control for Air-Breathing Hypersonic Vehicles. *IEEE Transactions on Industrial Electronics*, 2016; 63: 3038-3049.

[19] Li Z, Zhou W and Liu H. Nonlinear robust control of hypersonic aircrafts with interactions between flight dynamics and propulsion systems. *ISA Transactions*. 2016; 64: 1-11.

[20] Xu H, Mirmirani M and Ioannou P. Adaptive Sliding Mode Control Design for a Hypersonic Flight Vehicle. *Journal of Guidance, Control, and Dynamics*. 2004; 27: 829-38.

[21] Hu , Wu L, Hu C, et al. Adaptive sliding mode tracking control for a flexible air-breathing hypersonic vehicle. *Journal of the Franklin Institute*, 2012; 349: 559-577.

[22] Sun H, Li S and Sun C. Finite time integral sliding mode control of hypersonic vehicles. *Nonlinear Dynamics*. 2013; 73: 229-44.

[23] Zong Q, Wang J, Tian B, et al. Quasi-continuous high-order sliding mode controller and observer design for flexible hypersonic vehicle. *Aerospace Science and Technology*. 2013; 27: 127-37.

[24] Zong Q, Wang F, Tian B, et al. Robust adaptive dynamic surface control design for a flexible air-breathing hypersonic vehicle with input constraints and uncertainty. *Nonlinear Dynamics*. 2014; 78: 289-315.

[25] Xu B, Yang C and Pan Y. Global neural dynamic surface tracking control of strict-feedback systems with application to hypersonic flight vehicle. *IEEE transactions on neural networks and learning systems*. 2015; 26: 2563-75.

[26] Liu Z, Tan X, Yuan R, et al. Immersion and Invariance-Based Output Feedback Control of Air-Breathing Hypersonic Vehicles. *IEEE Transactions on Automation Science and Engineering*, 2016; 13: 394-402.

[27] Xu B, Zhang Q and Pan Y. Neural network based dynamic surface control of hypersonic flight dynamics using small-gain theorem. *Neurocomputing*. 2016; 173: 690-9.

[28] Gao H, Cai Y, Chen Z, et al. Offset-Free Output Feedback Robust Model Predictive Control for a Generic Hypersonic Vehicle. *Journal of Aerospace Engineering*. 2015; 28: 04014147.

[29] Zhao J, Zhou S and Zhou R. Distributed time-constrained guidance using nonlinear model predictive control. *Nonlinear Dynamics*. 2015; 84: 1399-416.

[30] Tao X, Li N and Li S. Multiple model predictive control for large envelope flight of hypersonic vehicle systems. *Information Sciences*. 2016; 328: 115-26.

[31] Bu X, Wu X, Zhang R, et al. Tracking differentiator design for the robust backstepping control of a flexible air-breathing hypersonic vehicle. *Journal of the Franklin Institute*. 2015; 352: 1739-1765.

[32] Su X and Jia Y. Constrained adaptive tracking and command shaped vibration control of flexible hypersonic vehicles. *IET Control Theory & Applications*. 2015; 9: 1857-68.

[33] Zong Q, Wang F, Tian B, et al. Robust Adaptive Approximate Backstepping Control Design for a Flexible Air-Breathing Hypersonic Vehicle. *Journal of Aerospace Engineering*. 2015; 28.

[34] An H, Liu J, Wang C, et al. Approximate Back-Stepping Fault-Tolerant Control of the Flexible Air-Breathing Hypersonic Vehicle. *IEEE/ASME Transactions on Mechatronics*. 2016; 21: 1680-1691.

[35] Wu G and Meng X. Nonlinear disturbance observer based robust backstepping control for a flexible air-breathing hypersonic vehicle. *Aerospace Science and Technology*. 2016; 54: 174-82.

[36] Xu B, Guo Y, Yuan Y, et al. Fault-tolerant control using command-filtered adaptive back-stepping technique: Application to hypersonic longitudinal flight dynamics. *International Journal of Adaptive Control and Signal Processing*. 2016; 30: 553-577.

[37] Banerjee S, Wang Z, Baur B, et al. $\mathscr{L}_1$ Adaptive Control Augmentation for the Longitudinal Dynamics of a Hypersonic Glider. *Journal of Guidance, Control, and Dynamics*. 2016; 39: 275-91.

[38] Bu X, Wu X, He G, et al. Novel adaptive neural control design for a constrained flexible air-breathing hypersonic vehicle based on actuator compensation. *Acta Astronautica*. 2016; 120: 75-86.

[39] Xu B, Sun F, Yang C, et al. Adaptive discrete-time controller design with neural network for hypersonic flight vehicle via back-stepping. *International Journal of Control*. 2011; 84: 1543-52.

[40] Xu B, Wang D, Sun F, et al. Direct neural discrete control of hypersonic flight vehicle. *Nonlinear Dynamics*. 2012; 70: 269-78.

[41] Gao D, Wang S, Zhang H. A Singularly Perturbed System Approach to Adaptive Neural Back-stepping Control Design of Hypersonic Vehicles. *Journal of Intelligent & Robotic Systems*. 2013; 73: 249-259.

[42] Yang F, Yuan R, Yi J, et al. Direct adaptive type-2 fuzzy neural network control for a generic hypersonic flight vehicle. *Soft Computing*. 2013; 17: 2053-2064.

[43] Poderico M, Morani G, Sollazzo A, et al. Fault-tolerant control laws against sensors failures for hypersonic flight. *18th AIAA/3AF International Space Planes and Hypersonic Systems and Technologies Conference*, 2012. AIAA 2012-5967.

[44] Gao M, Cai G and Nan Y. Robust adaptive fault-tolerant H_∞ control of reentry vehicle considering actu-

ator and sensor faults based on trajectory optimization. *International Journal of Control, Automation and Systems*. 2016; 14: 198-210.

[45] Saeid J, Petros I and Lael E. What is $\mathscr{L}_1$ Adaptive Control. *AIAA Guidance, Navigation, and Control Conference*. Boston, Massachusetts: 2013; American Institute of Aeronautics and Astronautics, AIAA-2013-4513.

[46] Hellmundt F, Wildschek A, Maier R, et al. Comparison of $\mathscr{L}_1$ Adaptive Augmentation Strategies for a Differential PI Baseline Controller on a Longitudinal F16 Aircraft Model. *Advances in Aerospace Guidance, Navigation and Control*. Springer International Publishing, 2015; p.99-118.

[47] Hovakimyan N and Cao C. $\mathscr{L}_1$ *adaptive control theory : guaranteed robustness with fast adaptation*. Philadelphia: Society for Industrial and Applied Mathematics, 2010.

[48] Lei Y, Cao C, Cliff E, et al. Design of an $\mathscr{L}_1$ Adaptive Controller for Air-breathing Hypersonic Vehicle Model in the Presence of Unmodeled Dynamics. *AIAA Guidance, Navigation and Control Conference and Exhibit*. South Carolina, 2007; AIAA-2007-6527.

[49] Prime Z, Doolan C, and Cazzolato B. Longitudinal $\mathscr{L}_1$ Adaptive Control of a Hypersonic Re-Entry Experiment. *15th Australian International Aerospace Congress*, Melbourne, VIC, 2013. pp.717-726.

[50] Li Z and Hovakimyan N. $\mathscr{L}_1$ adaptive controller for MIMO systems with unmatched uncertainties using modified piecewise constant adaptation law. *51st IEEE Conference on Decision and Control*. Hawaii, USA, 2012, pp.7303-8.

[51] Parker J, Serrani A, Yurkovich S, et al. Control-Oriented Modeling of an Air-Breathing Hypersonic Vehicle. *Journal of Guidance, Control, and Dynamics*. 2007; 30: 856-69.

[52] Bolender M, Doman D. Nonlinear Longitudinal Dynamical Model of an Air-Breathing Hypersonic Vehicle. *Journal of Spacecraft and Rockets*. 2007; 44: 374-387

[53] Tony A, Zhu J, Michael B, et al. Flight Control of Hypersonic Scramjet Vehicles Using a Differential Algebraic Approach. *AIAA Guidance, Navigation, and Control Conference and Exhibit*, Keystone, Colorado, Aug. 21-24, 2006. AIAA-2006-6559.

[54] Xu B, Shi Z, Yang C, et al. Neural control of hypersonic flight vehicle model via time-scale decomposition with throttle setting constraint. *Nonlinear Dynamics*. 2013; 73: 1849-61.

[55] Leman T, Xargay E, Dullerud G, et al. $\mathscr{L}_1$ Adaptive Control Augmentation System for the X-48B Aircraft. *AIAA Guidance, Navigation, and Control Conference, Guidance, Navigation, and Control and Co-located Conferences*, Chicago, Illinois, 2009. AIAA-2009-5619.

6. Contact Author Email Address

Chen Qi: skywalkerchen@live.com

7. Copyright Statement